The Journal of Experimental Biology 214, 1571-1585

doi:10.1242/jeb.051623

RESEARCH ARTICLE

Failure by fatigue in the field: a model of fatigue breakage for the macroalga *Mazzaella*, with validation

Katharine J. Mach*, Sarah K. Tepler, Anton V. Staaf, James C. Bohnhoff and Mark W. Denny

Hopkins Marine Station of Stanford University, Pacific Grove, CA 93950, USA

*Author for correspondence (mach@stanford.edu)

Accepted 24 January 2011

SUMMARY

Seaweeds inhabiting the extreme hydrodynamic environment of wave-swept shores break frequently. However, traditional biomechanical analyses, evaluating breakage due to the largest individual waves, have perennially underestimated rates of macroalgal breakage. Recent laboratory testing has established that some seaweeds fail by fatigue, accumulating damage over a series of force impositions. Failure by fatigue may thus account, in part, for the discrepancy between prior breakage predictions, based on individual not repeated wave forces, and reality. Nonetheless, the degree to which fatigue breaks seaweeds on wave-swept shores remains unknown. Here, we developed a model of fatigue breakage due to wave-induced forces for the macroalga *Mazzaella flaccida*. To test model performance, we made extensive measurements of *M. flaccida* breakage and of wave-induced velocities experienced by the macroalga. The fatigue-breakage model accounted for significantly more breakage than traditional prediction methods. For life history phases modeled most accurately, 105% (for female gametophytes) and 79% (for tetrasporophytes) of field-observed breakage was predicted, on average. When *M. flaccida* fronds displayed attributes such as temperature stress and substantial tattering, the fatigue-breakage model underestimated breakage, suggesting that these attributes weaken fronds and lead to more rapid breakage. Exposure to waves had the greatest influence on model performance. At the most wave-protected sites, the model underpredicted breakage, and at the most wave-exposed sites, it overpredicted breakage. Overall, our fatigue-breakage model strongly suggests that, in addition to occurring predictably in the laboratory, fatigue-induced breakage of *M. flaccida* occurs on wave-swept shores.

Key words: fatigue, breakage, wave forces, *Mazzaella*, macroalgae, biomechanics, ecomechanics.

INTRODUCTION

Wave-swept rocky shores present organisms with physical rigors associated with tides and waves. At low tide, organisms experience potentially large temperature fluctuations and desiccation (Denny and Wethey, 2001; Tomanek and Helmuth, 2002). At high tide, hydrodynamic forces exerted on organisms by breaking waves may be extreme: wave-induced velocities frequently reach 5–10 m s^{-1} and at some sites exceed 35 m s^{-1} (Gaylord, 1999; Denny and Gaylord, 2002). These wave-associated velocities represent some of the harshest physical conditions on earth; water traveling at 2 m s^{-1}, a relatively mild velocity for the intertidal region, imposes as much force as hurricane-speed winds blowing at 130 m.p.h. (~209 km h^{-1}).

Intertidal macroalgae, tethered to a rock, experience wave-induced velocities in full. Macroalgae attach to a rock through a holdfast, from which one or several fronds emerge. Fronds assume various morphologies, and a typical construction includes a stem-like stipe and fleshy blade(s). The holdfast and frond(s) together constitute a thallus. Breakage and dislodgment of macroalgal thalli commonly occurs as waves break repeatedly over intertidal rocks: up to 10–90% of intertidal and shallow subtidal populations may break or dislodge during wintertime storms (e.g. Hansen and Doyle, 1976; Foster, 1982; Seymour et al., 1989; Dudgeon and Johnson, 1992; Dudgeon et al., 1999; Dyck and DeWreede, 1995; Dyck and DeWreede, 2006a; Dyck and DeWreede, 2006b). For most seaweeds, such breakage soon translates into death for dislodged portions of thalli. Indeed, dislodged thalli and frond fragments form important carbon and nitrogen sources in coastal and nearshore environments (e.g. Rossi and Underwood, 2002; Dugan et al., 2003; Orr et al., 2005; Liebezeit et al., 2008; Lastra et al., 2008).

Nonetheless, biomechanical models of macroalgal breakage have frequently underestimated, and sometimes greatly underestimated, breakage of seaweeds due to wave-imposed forces. The traditional approach has involved determination of a seaweed's breaking strength and comparison of this strength with maximal wave-induced force, with breakage often under-predicted (Koehl and Alberte, 1988; Gaylord et al., 1994; Johnson and Koehl, 1994; Friedland and Denny, 1995; Utter and Denny, 1996; Denny et al., 1997; Johnson, 2001; Kitzes and Denny, 2005). Researchers have suggested that other factors, such as damage due to herbivory, abrasion or physiological stressors, may account for observed breakage rates, weakening fronds that individual waves then break (Friedland and Denny, 1995; Utter and Denny, 1996; Kitzes and Denny, 2005; Denny, 2006).

Additionally, researchers have investigated the possibility that seaweeds break not just from large individual wave-imposed forces but from damage accumulated over a series of wave-imposed forces (Hale, 2001; Mach et al., 2007a; Mach et al., 2007b; Mach, 2009). Over 8000 waves break onshore each day, and the resulting repetitive nature of wave-imposed loadings may have a bearing on macroalgal failure. Hale (Hale, 2001) and Mach and colleagues (Mach et al., 2007b) found that cracks introduced into macroalgal blades can increase in length in conditions of repeated loadings and

eventually cause specimen fracture. Mach (Mach, 2009) then documented that the entire process of fatigue failure, from the formation of small cracks through their growth to the point of specimen rupture, occurs predictably in the seaweed *Mazzaella*. It has thus been established that flat-bladed seaweeds fail by fatigue in standard laboratory loading conditions. However, the degree to which fatigue breaks macroalgal fronds in the field remains unknown.

The present study addresses this gap in understanding, assessing failure by fatigue on wave-swept shores. First, a model of breakage by fatigue in *Mazzaella flaccida* was developed. Second, breakage of *M. flaccida* was tracked in the field for 11 months. Third, breakage predicted by the model was compared with breakage measured in the field to assess the performance of the fatigue model and the degree to which *M. flaccida* fails by fatigue in natural populations. Fatigue-model predictions were compared with traditional predictions of maximal-force breakage, and other influences on fatigue-model predictions, such as temperature stress and the presence of endophytes and reproductive tissue, were assessed.

A simple numerical model of fatigue breakage in *M. flaccida*

Wave-induced velocities

Linear wave theory has been used to approximate water velocities associated with breaking waves (Denny, 1988; Denny, 2006). In the intertidal region, however, topographical features can amplify or diminish water velocities as compared with waveform velocities predicted from linear wave theory (Denny et al., 2003; Denny, 2006). As a result, to accurately represent water velocities occurring at a given intertidal site, empirical measurements must be made. Helmuth and Denny found that maximal wave-imposed forces and velocities can be correlated with offshore significant wave height, which is a measure of ocean swell conditions equal to the mean height of the highest third of waves (Helmuth and Denny, 2003). Most sites they studied (130 of 221) displayed a significant and substantial asymptotic relationship between offshore significant wave height and maximal wave-induced velocity (or, equivalently, maximal wave-induced force), with velocity increasing non-linearly towards a defined limit as wave height increased. Accordingly, maximal wave-imposed velocity, u_{max} ($m\,s^{-1}$), at such sites can be related to offshore significant wave height, H_S, as:

$$u_{max} = u_{asym}\,[1 - \exp\,(-H_S / H_K)]\,, \quad (1)$$

where u_{asym} is the asymptotic maximal velocity and H_K is the offshore significant wave height above which wave-imposed velocity is within 37% (=1/*e*) of u_{asym}. Helmuth and Denny also found that, at a handful of sites (16 of 221), maximal velocity increased with significant wave height without an apparent upper bound (Helmuth and Denny, 2003). At such sites, u_{max} can be expressed as a linear function of H_S:

$$u_{max} = a\,H_S\,, \quad (2)$$

where a is a fitted constant.

Hydrodynamic forces

The primary force exerted on seaweeds exposed to breaking waves is drag (N) (Gaylord et al., 1994; Gaylord, 2000; Boller and Carrington, 2006a). For the high velocities of intertidal wave-induced flows, drag force, F_D, can be modeled by this relationship:

$$F_D = 1/2\;\rho\;A\;C_D\;u^2\,, \quad (3)$$

where ρ is fluid density ($kg\,m^{-3}$), here seawater density; A is a representative area (m^2), here of a *M. flaccida* frond; C_D is a dimensionless drag coefficient, which varies with frond shape and with frond reconfiguration occurring with increasing water velocity (e.g. Vogel, 1984; Carrington, 1990; Boller and Carrington, 2006b); and u is water velocity ($m\,s^{-1}$), here of wave-induced flows associated with breaking waves.

Corresponding stress due to drag, S_D (Pa) is drag force normalized by the cross-sectional area of the frond resisting drag, A_{xs} (m^2):

$$S_D = F_D / A_{xs}\,. \quad (4)$$

Fatigue damage

Fatigue behavior of *M. flaccida* has been quantified previously with standard laboratory measurement techniques (Mach, 2009). In the approach employed, each blade specimen was extended to a given tensile force and then relaxed to 0 N, repeatedly, until the specimen broke. Tests ranged in duration from a few loading cycles to over 1 million loadings. From these measurements, the number of loading cycles required for breakage of blade specimens, N_{br}, was related to maximal stress imposed in each cycle, S_{max} (Pa):

$$\log S_{max} = m\,\log N_{br} + b\,, \quad (5)$$

where m and b are fitted constants. Note that when N_{br}=1 the corresponding S_{max} is equivalent to breaking strength as traditionally measured by extending *Mazzaella* specimens in tension continuously until rupture occurs.

Given this quantification of fatigue behavior, Miner's rule (Miner, 1945; Shigley and Mischke, 2001) can be used to sum fatigue damage of *M. flaccida* over a series of loadings and to determine thereby whether the series of loadings is sufficient to cause breakage. Damage for a given loading cycle, D_{cy}, can be expressed as:

$$D_{cy} = 1 / N_{br,cy}\,, \quad (6)$$

where $N_{br,cy}$ is the number of cycles required for breakage at the maximal stress imposed in the loading cycle. For a series of loading cycles, fatigue damage can be summed to determine the total fatigue damage, D_{tot}, incurred due to the loadings:

$$D_{tot} = \Sigma D_{cy}\,. \quad (7)$$

Most basically, failure over the course of a loading series is predicted when D_{tot} equals or exceeds 1. If D_{tot} is less than 1, the loading series is not predicted to cause failure. Because Eqn 5 describes failure due to individual as well as repeated loading cycles, breakage predicted through Eqn 7 also encompasses breakage due to individual as well as repeated loadings.

For wave-imposed flows relevant to fatigue breakage of *M. flaccida*, each wave imposes on a frond the equivalent of one loading cycle, with stress in a frond increasing from 0 Pa to maximal stress corresponding to the maximal velocity associated with the breaking wave; previous determination of *M. flaccida* fatigue behavior involved loadings with minimum stress also of 0 Pa, to mimic wave-induced loadings (Mach, 2009). For each wave-imposed loading, use of Eqns 3 and 4 allows determination of maximal wave-induced stress from maximal wave-associated velocity. Then, Eqns 5 to 7 facilitate assessment of fatigue damage of a *M. flaccida* frond due to maximal stresses imposed by a series of wave loadings.

MATERIALS AND METHODS

The study species: *M. flaccida*

Mazzaella is a red macroalga (phylum Rhodophyta) with flat-bladed morphology. *Mazzaella* was chosen previously for determination of fatigue behavior because its blades are amenable to preparation of test specimens, repeated-loading testing and documentation of

fatigue-crack formation (Mach, 2009). This study focused on *M. flaccida* (Setchell and Gardner), one of two *Mazzaella* species for which fatigue behavior was established. *Mazzaella flaccida* grows intertidally from Alaska to Point Conception, CA, USA, with populations following points of upwelling through Northern Baja California, Mexico (Abbott and Hollenberg, 1976). The life history of *M. flaccida* is triphasic. The haploid gametophyte phase comprises male and female gametophyte thalli; after fertilization, a microscopic diploid carposporophyte phase, which is not free living, forms within the blades of female gametophyte thalli, generating diploid spores that give rise to a tetrasporophyte phase. The tetrasporophyte, morphologically similar to the gametophytes, produces meiotic spores that develop into gametophytes. Fatigue behavior was assessed for male gametophytes, female gametophytes and tetrasporophytes of *M. flaccida* collected at Hopkins Marine Station (HMS), Pacific Grove, CA, USA (Mach, 2009), and the present study examines field breakage of the same population of *M. flaccida*.

Study sites

Breakage of *M. flaccida* was monitored at 10 sites at HMS. In order to minimize potential variation in breakage correlated with tidal height, the sites were selected to each span a similar tidal range. From the overall *M. flaccida* tidal range of 0.24 to 1.85 m above mean lower low water (MLLW; National Tidal Datum Epoch 1983–2001, Monterey, CA, USA; tidal range measured in October 2008, with a Topcon Electronic Total Station, Topcon America Corporation, Paramus, NJ, USA; GTS-211D), 20 possible sites were located, each centered on a tidal height from 0.6 to 1.1 m above MLLW.

From 20 potential sites, 10 were randomly selected for use. In the central region of each of these 10 study sites, a hole of 5.1 cm in diameter, widened to 10 cm diameter at the rock surface, and approximately 14 cm in depth was drilled in the granite intertidal rock, using a pneumatic drill and portable air compressor. Into this widened upper portion, a threaded collar for securing wave-recording devices was installed using marine epoxy (Splash Zone Epoxy 788, Z-Spar Coatings, Kop-Coat Inc., Pittsburgh, PA, USA). Centers of the 10 threaded collars had tidal heights ranging from 0.76 to 1.09 m above MLLW, with a mean height ±s.d. of 0.94±0.09 m above MLLW. Following labeling of plants at each site, described below, the tidal height range spanned by labeled *M. flaccida* thalli was also measured for each site.

Tagging of thalli

At the 10 sites, *M. flaccida* thalli were each labeled non-invasively with a piece of marine epoxy affixed to the rock next to the holdfast, into which a plant number and an arrow were etched to identify the holdfast. Occasionally, over the course of the monitoring period, epoxy labels were dislodged by wave-induced forces. In such cases, label location was determined from the photographic record described below, and the dislodged label was replaced with an identical new one.

Thalli were initially labeled on 12 April 2009. At that time, 8–9 thalli were labeled at each of the 10 sites, with the exception of one site at which only 3 thalli were present and thus labeled, with more plants labeled subsequently. By May, the number of labeled thalli was increased to at least 18 per site at all but two sites. By June, the remaining two sites also had 18 thalli.

As necessary when thalli were dislodged by waves, new thalli were labeled at each site to maintain at least 18 thalli at each wavelogger site at all times. Following winter storms, however, it eventually became impossible to maintain 18 thalli at some sites where substantial dislodgment of thalli occurred. At such sites, thalli number was maintained as near 18 per site as possible.

Tagged *M. flaccida* thalli, across the 10 sites, ranged overall in tidal height from 0.51 to 1.33 m above MLLW. Across sites, the lower limits of *M. flaccida* thalli ranged from 0.51 to 0.95 m above MLLW, with a mean lower-limit height ±s.d. of 0.77±0.12 m above MLLW. The upper limits of *M. flaccida* thalli ranged from 0.90 to 1.33 m above MLLW, with a mean upper-limit height ±s.d. of 1.13±0.13 m above MLLW.

Monitoring of thalli

Tagged thalli were monitored for 11 months, from April 2009 to February 2010. During the lowest tides of every 2 week tidal cycle, a series of measurements was made for all tagged thalli. For each thallus, reproductive status (reproductive or not) and life history phase were noted, and the number of fronds with length greater than 1 cm was estimated, primarily for use in locating thalli following tag dislodgment. Only tetrasporophyte and female gametophyte thalli could be visually identified to life history phase in the field. For any thallus that appeared to be a male gametophyte, a small portion of a short frond within the thallus was taken to the laboratory for sectioning to verify life history phase identity. For some thalli, life history phase remained unknown because, for example, a thallus was dislodged before any of its fronds developed reproductive structures.

Dimensions of the longest frond in each thallus were documented every tidal cycle. The length of each longest frond, from the base of the stipe (where it joined the holdfast) to the tip of the blade was determined, along with the maximal width of the blade and the width of the blade base, just above the stipe and apophysis (where the apophysis is the broadening region between the stipe and the blade). Length was measured to the nearest 0.1 cm, and maximal and base widths were determined to 0.5 cm, always rounding up. Additionally, if the frond was tattered such that blade width was most narrow at a location other than the base, where breakage seemed likely, this non-base, vulnerable-to-breakage width was also noted, again rounding up to the nearest 0.5 cm. From one measurement period to the next, breakage for a thallus was considered to have occurred if the length of the longest frond in the thallus decreased by 1 cm or more.

Also, seven attributes of the longest frond in each thallus were evaluated: reproductive structures, bleaching, tattering, holes, herbivore markings, endophytes and epiphytes. The presence of reproductive structures and holes was quantified on a scale from 0 to 5, and the other attributes were assessed on a scale of 0 to 4. For all 7 categories, 0 indicated the absence of the attribute: no reproductive structures present in the longest frond, no bleaching present, etc. The maximal value of 4 or 5 indicated complete coverage by the attribute: the whole blade surface covered with fully developed reproductive structures, entire frond bleached, etc. ‘Tattering’ was defined as damage to a blade that originated from or extended to a blade margin (e.g. a tear extending from the blade margin to the blade center), while ‘holes’ were defined as damage confined to the interior portion of a frond (e.g. a circular hole in a blade).

Thalli were usually photographed monthly, during every other tidal-cycle measurement series. In cases of tag dislodgment or emergence of a new thallus next to a tagged one, these photographs ensured correct identification of thalli.

Breakage of fronds was characterized generally by plotting the overall breakage rates for thalli and breakage rates for each life

history phase over the 11 month study. Additionally, breakage as a function of frond size was evaluated for each life history phase through ANOVA analyses, plus one Kruskal–Wallis test (JMP®, version 4.0.4, SAS Institute, Cary, NC, USA). Trends in largest frond size and reproductive status were also assessed.

Temperature measurements at study sites

From June 2009 to February 2010, temperature was measured at each of the 10 sites. Every tidal cycle, a Thermochron® iButton® temperature logger (Maxim Integrated Products, formerly Dallas Semiconductor, Sunnyvale, CA, USA) was deployed at each site within a spherical brass finial painted black with nail polish. The loggers recorded temperature every 15 min during each approximately 2 week-long deployment. To compare maximal temperature across deployment periods, peak temperature measurements at each site were averaged for each deployment.

Wave-induced velocity measurements at study sites

Two device types were used to record wave-induced forces. In both cases, devices were deployed in the central hole at each of the 10 sites, with a roughened sphere protruding from the surface of the rock.

When possible, continually recording force sensors were deployed. These battery-powered loggers recorded data to internal microSD card storage with an AVR atmega644p processor (Atmel, San Jose, CA, USA). Using US-06002 force transducers (Bokam Engineering Inc., Santa Ana, CA, USA), two-axis force measurements on a roughened plastic sphere with diameter of 1.9 cm were recorded 100 times per second. Device temperature and battery status measurements were recorded once every 2 s, and sensor conditioning was performed by two MAX4208 differential amplifiers (Maxim Integrated Products, Sunnyvale, CA, USA). The devices consisted of a modular stack of printed circuit boards and two TL-5104 batteries (Tadiran, Lake Success, NY, USA). Devices were deployed in custom-made waterproof housings, and deployment time for loggers, restricted by battery life, was typically 10–15 days of continuous sampling. Additional information and development details can be found at http://code.google.com/p/wavelogger/.

The number of continually recording sensors deployed across the sites fluctuated throughout the study as loggers went in and out of repair. Over the course of the 11 months of thalli measurements, functioning continually recording sensors were rotated across the 10 sites, so that continual sampling occurred at each site. For sites lacking continually recording sensors at any given time, spring-scale dynamometers (Bell and Denny, 1994; Helmuth and Denny, 2003) were used instead. Over the course of deployment, each dynamometer recorded the maximal force exerted on a Wiffle golf ball with a diameter of 4.1 cm. Deployments most often lasted 1–2 days, but could be as long as 2 weeks.

For both devices, drag force imposed on the protruding, roughened spheres was converted to equivalent water velocity through the use of Eqn 3. Area A was the maximal cross-sectional area of the device's sphere, and C_D was measured previously for the roughened spheres as a function of Reynolds number, Re:

$$\log_{10} C_D = 0.6761 (\log_{10} Re)^3 - 10.907 (\log_{10} Re)^2 + 58.183 (\log_{10} Re) - 103.1 , \quad (8)$$

where Re for device spheres is given by:

$$Re = u d / \nu , \quad (9)$$

where u again is velocity (m s^{-1}), d is sphere diameter (m) and ν is kinematic viscosity (m^2 s^{-1}), here of seawater.

Measurements for fatigue-breakage model

To compare *M. flaccida*'s actual breakage, monitored in the field study, with breakage predicted by the fatigue model for each monitored frond, measurements were first made as necessary for Eqns 1–7.

Frond area relevant to drag

Area A required for Eqn 3 is the single-sided surface area of a frond. Measuring A for the longest frond of each tagged thallus during every tidal cycle, however, was not feasible. Instead, length, L, and maximal width, W, of the longest frond in each tagged thallus were measured in the field every tidal cycle. Then, the relationship between A and the product of L and W was used to approximate A from measured frond dimensions.

To determine this relationship, on two separate dates, 6 July and 22 September 2009, *M. flaccida* fronds (N=288 in total) were collected from intertidal rocks at HMS, away from the study sites, and brought into the laboratory. For each blade, life history phase was determined if reproductive tissue was present, with tetrasporophytes and female gametophytes identified visually and male gametophytes sectioned and examined under the microscope. Maximal frond length L and maximal blade width W were measured as in field surveys of tagged thalli. Additionally, each frond was flattened with small black weights and photographed against a white background. From this photograph, single-sided surface area A was calculated in ImageJ (Research Services Branch, National Institute of Mental Health, Bethesda, MD, USA, version 1.37). Effects of life history phase on the relationship between A and the product of L and W were assessed with ANCOVA analyses (JMP®). Then, for all fronds, the product of L and W was plotted against measured area A on logarithmic axes to yield uniform variance of residuals along the best-fit regression line. The regression line equation and the standard deviation of residuals were then used to approximate A from measured frond dimensions in the fatigue-breakage model.

Mazzaella flaccida drag coefficients

Drag coefficient C_D, also required for determining drag force through Eqn 3, was determined previously for *M. flaccida* as a function of water velocity u (Mach, 2009). The relationship found in that study was used here for $u \leq 9.5$ m s^{-1}: $C_D = 0.0793\, u^{-0.7565}$. Additionally, for $u \leq 9.5$ m s^{-1}, the standard deviation of residuals was determined as a function of u. For $u > 9.5$ m s^{-1}, C_D=0.01444 was employed, to avoid inaccuracies of extrapolating C_D beyond tested u (Carrington, 1990; Boller and Carrington, 2006b).

Frond cross-sectional area

For determining stress due to drag, S_D, through Eqn 4, cross-sectional area A_{xs} was approximated for each longest frond measured in surveys of tagged thalli. Blades of *M. flaccida* are most susceptible to breakage at the base, above the stipe and apophysis, the location at which drag forces are greatest and cross-sectional areas resisting this force are relatively small. In the field surveys of longest fronds in tagged thalli, blade width at the base was measured. This blade width was multiplied by approximate frond thickness to determine A_{xs} for Eqn 4. For this calculation, frond thickness as measured previously (Table 1) (Mach, 2009) was used. For tattered fronds that had a vulnerable-to-breakage width narrower than the blade width at the base, this narrower width was used in calculating A_{xs}.

Fatigue behavior

Fatigue behavior, as determined previously for *M. flaccida* specimens loaded repeatedly at 1 Hz (Mach, 2009), was used for

Table 1. Characteristics of *Mazzaella flaccida* measured previously

Life history phase	Thickness (mm, mean ± s.d)	*N*	*m*	*b*	*N*	Pull-to-break strength (MPa, mean ± s.d.)	*N*
Female gametophytes	0.553±0.103	67	–0.078	6.102	42	1.88±0.70	17
Tetrasporophytes	0.466±0.061	70	–0.087	6.264	43	2.16±0.39	17
Male gametophytes	0.376±0.053	62	–0.077	6.394	44	3.18±0.51	17
M. flaccida overall	0.468±0.104	199	–0.068	6.212	129	2.41±0.78	51

Data are from Mach, 2009: frond thickness; fitted constants *m* and *b* for specimens loaded repeatedly at 1 Hz; and pull-to-break strengths. Sample size *N* is given for these thickness, fatigue and pull-to-break strength measurements.

the fatigue-breakage model in this study. For Eqn 5, fitted constants *m* and *b* are given in Table 1. In addition, standard deviations of residuals were calculated for each regression for use in the model.

Using the fatigue-testing methods described in Mach (Mach, 2009), a final series of fatigue tests was performed to ensure the validity of comparing continuous repeated loading, as performed in the 1 Hz testing summarized above, with repeated loading due to breaking waves, for which loadings are imposed approximately every 10 s. From August to November 2008, *M. flaccida* specimens were prepared and tested at HMS using protocols outlined in Mach (Mach, 2009). All loadings were again stress controlled and sinusoidal in profile, but each loading lasting 1 s was followed by a period of no loading for 9 s, roughly approximating loadings imposed on *M. flaccida* by breaking waves. Female gametophyte (*N*=20), tetrasporophyte (*N*=21) and male gametophyte (*N*=20) fronds were tested. Fatigue failure was again characterized with log–log plots of loading stress *versus* number of cycles to breakage, and linear regressions were fitted to these plots. Data for specimens loaded with pauses between loadings were then compared with data collected previously (Mach, 2009) for specimens loaded at 1 Hz without pauses, using ANCOVA analyses (JMP®).

Pull-to-break strengths

With the model's simulations, breakage predicted by fatigue was compared with breakage as traditionally assessed, breakage based on pull-to-break strength. Pull-to-break strengths of *M. flaccida* blades were measured by Mach (Mach, 2009) and employed here (Table 1).

For comparison, pull-to-break strengths were also determined by testing *M. flaccida* in the field as has been done previously for other *Mazzaella* species (Shaughnessy et al., 1996). Pull-to-break testing of *M. flaccida* in the field occurred on 2–3 November 2009. For tetrasporophyte (*N*=50), female gametophyte (*N*=50) and male gametophyte (*N*=50) fronds, the blade of each frond was folded over a rubber-coated strip of aluminium and clamped with rubber-lined alligator clips, which were attached by string to a spring scale (Pesola® Medio-Line Spring Scale, Forestry Suppliers Inc., Jackson, MS, USA; 2500 g). Attached as such to a frond, the spring scale was smoothly pulled approximately parallel to the substratum, for about 1.5 s, until breakage occurred. Break location was noted (blade, stipe, stipe–holdfast junction, holdfast, or substratum), along with force required for breakage and frond width and thickness at the location of breakage. Breaking force and stress were compared across life history phases with ANOVA analyses (JMP®).

Maximal wave-induced velocities

For Eqns 1 and 2, the relationship between offshore significant wave height H_S and maximal onshore wave-induced water velocity u_{max} was determined for each of the 10 sites.

H_S was measured every 20 min by the Cabrillo Point Buoy (Datawell Directional Buoy, Coastal Data Information Program, Scripps Institution of Oceanography, La Jolla, CA, USA; Station 158: 36°37.58′N, 121°54.43′W), located approximately 0.5 km offshore from the study sites. Maximal wave-induced water velocities were determined from the spring-scale dynamometers and the continually recording force sensors deployed at the sites.

Force data from the dynamometers were processed through previously used methods (Helmuth and Denny, 2003): for a given deployment, maximal H_S from the buoy and u_{max} from the dynamometer were determined. Force data from the continually recording sensors were processed similarly, with u_{max} determined from each day of recorded force data and corresponding maximal H_S retrieved from buoy records. With data from the dynamometers and continual force sensors, u_{max} was determined as a function of H_S for each of the 10 sites, and data were fitted with Eqns 1 and 2. For each site, R^2 values for Eqns 1 and 2 were compared, and the regression with higher R^2 was chosen to describe the site in the fatigue-breakage model. Standard deviations of residuals around chosen regressions were calculated for all sites.

Non-maximal wave-induced velocities

The fatigue-breakage model required estimation not only of maximal wave-induced velocity in a given period but also of all the other non-maximal wave-induced velocities. Force data from the continually recording sensors were processed to determine the distribution of wave-induced velocities below maximal velocities.

First, for each day (*N*=461) of force data recorded at the study sites, peak force every 10 s was determined, yielding 8640 peak forces per day of recorded data. Waves break onshore approximately every 10 s, so this first processing step on average determined peak force imposed per breaking wave. Peak forces were determined without regard to tidal height, so effects of tidal height on peak forces experienced at the *M. flaccida* sites were included in this step. Second, each peak force was converted into an equivalent peak wave-induced water velocity ($m\,s^{-1}$). Third, the maximal peak velocity ($m\,s^{-1}$) for each day of recorded data, $u_{p,max}$, was determined, and each peak velocity that day, u_p, was normalized by $u_{p,max}$:

$$u_{p,norm} = u_p / u_{p,max} . \quad (10)$$

Fourth, the distributions of normalized peak velocities $u_{p,norm}$ were analyzed. Cumulative probability distributions of $u_{p,norm}$ were generated for each day of recorded data, excluding days (*N*=62) for which $u_{p,max}<5\,m\,s^{-1}$. This $u_{p,max}$ threshold excluded days for which the sensitivity limit ($u\approx0.8\,m\,s^{-1}$) of the sensors greatly influenced the distribution of $u_{p,norm}$. A mean cumulative probability distribution was calculated for all days of recorded data, and a probability density function of $u_{p,norm}$ was approximated from this mean cumulative probability distribution. Finally, an overall frequency histogram of all $u_{p,norm}$ (*N*=3,447,360) was determined for days for which $u_{p,max}\geq5\,m\,s^{-1}$.

Implementation of field-breakage model

For all *M. flaccida* thalli tracked in the field, measured breakage was compared with breakage predicted by the fatigue model. For

each tagged thallus tracked over the 11 month field study, breakage for a thallus was defined as the longest frond decreasing in length by 1 cm or more over the 2 week period between measurements. Through field measurements every 2 weeks, breakage was thus known to occur or not for the longest frond of each tagged thallus. The overall question then was: how well does the fatigue-breakage model predict this breakage?

For each tagged thallus for each 2 week period, the model predicted whether the longest frond in the thallus would break by fatigue. The basic unit of prediction for the model was therefore a tagged thallus's longest frond, with known dimensions, attributes and actual breakage outcome for the 2 week period. Overall, there were 3122 'basic units' for prediction, or 3122 fronds with 2 week period measurements: 1019 female gametophytes, 1262 tetrasporophytes, 525 male gametophyes and 316 fronds with unknown life history phase.

The model's predictions proceeded as follows. First, a hypothetical 2 week series of wave-associated velocities was generated for each longest frond, spanning from one measurement period to the next. For the given 2 week period, offshore significant wave height H_S was known from the offshore buoy, measured every 20 min. For each 20 min period, H_S was then converted to maximal onshore wave-induced water velocity u_{max}, using the appropriate fitted regression (Eqn 1 or 2) for the site and then sampling randomly around the regression from a normal distribution with standard deviation equal to the calculated standard deviation of the residuals. To determine all of the peak wave-induced velocities in the 20 min period, every 10 s a normalized peak velocity $u_{p,norm}$ was randomly selected from the 3,447,360 normalized peak velocities from the continual force sensors. Multiplying each randomly selected $u_{p,norm}$ by u_{max} for the corresponding 20 min period yielded a hypothetical series of wave-induced velocities for the frond.

Second, given this hypothetical series of wave-induced velocities, the fatigue damage for the longest frond being assessed was determined, through the use of Eqns 3–7. If the total fatigue damage D_{tot} incurred in the frond's blade for the hypothetical series of wave-induced loadings equaled or exceeded 1, the model predicted breakage by fatigue would occur. In brief, the calculations proceeded as follows. For each longest frond with its hypothetical 2-week series of wave-induced velocities, predictions of fatigue damage were made iteratively, 51 times per longest frond, to incorporate various sources of variability. The final model prediction for each frond, breakage by fatigue or no breakage by fatigue, was simply whichever outcome was predicted more often (26 or more times) by the model. For each of the 51 iterations for a frond, each peak velocity >0.8 m s^{-1} was converted to drag F_D (Eqn 3) and stress due to drag S_D (Eqn 4) using measurements described in the section above and appropriately sampling from the variability around these measurements. Then, with Eqns 5 and 6, fatigue damage D_{cy} for each peak velocity was determined, using known fatigue behavior for each life history phase (described above) and sampling appropriately around each regression. Summing D_{cy} across the 2 week series of velocities yielded an estimate of D_{tot} and therefore a prediction of fatigue breakage or not for the frond iteration. Simultaneously for each frond iteration, maximal stress due to drag S_D over the 2 week velocity series was compared with measured pull-to-break strengths, for which variability was again sampled, to yield a prediction of breakage as traditionally done, considering only pull-to-break failure and not also incorporating effects of repeated loading as in the fatigue predictions. As a final note on model implementation, wherever measurements incorporated into the model were specific to life history phase, mean *M. flaccida* measurements and corresponding variability were used for fronds of unknown life history phase.

Model performance was assessed through comparing, for the different life history phases, the number of longest fronds predicted by the model to break with the number of longest fronds that actually broke for each 2 week tidal cycle. This ratio of predicted-to-actual frond breakage was compared across categories of the various quantified frond attributes (e.g. bleaching and endophytes) and across the 10 sites. ANOVA and Kruskal–Wallis analyses (JMP®) and *t*-tests (Microsoft® Excel) were used to assess the outcome of these comparisons.

RESULTS

Trends in length and breakage of tagged thalli

Longest-frond length varied for tagged thalli over the course of field surveys from April 2009 to October 2010 (Fig. 1). From spring to summer, longest fronds increased in length for thalli of each life history phase and for thalli of unknown life history phase; from autumn to winter, longest fronds decreased in length (Fig. 1). Overall, fronds were longest for male gametophyte thalli (Fig. 1C) and shortest for thalli of unknown life history phase (Fig. 1D).

For the two life history phases for which reproductive status could be easily and non-invasively assessed in the field (female gametophytes and tetrasporophytes), the presence of reproductive fronds in thalli followed similar trends (Fig. 2). For both life history stages, the fraction of tagged thalli with visible reproductive structures generally increased from spring to summer, with some decrease into winter (Fig. 2). Additionally, the fraction of thalli with visible reproductive structures was greater for the larger size classes.

Breakage, defined as the longest frond in a given thallus decreasing in length by 1 cm or more from one tidal-cycle measurement to the next, varied over the course of field surveys (Fig. 3). The percentage of thalli exhibiting longest-frond breakage varied from 10 to 47% for all fronds (Fig. 3A) and from 3 to 53% for individual life history phases (Fig. 3B–D). In general, the percentage breakage was lower in spring and summer than in fall and winter.

The percentage breakage for thalli of each life history phase and for thalli of unknown life history phase was averaged over all tidal-cycle measurements for each of three longest-frond size classes: length of 0–10, 10–20 and 20–35 cm (Fig. 4). If a given life history phase had fewer than two fronds in a size class for a given tidal-cycle measurement, that tidal-cycle measurement for the size class and life history phase was excluded from the mean. For thalli of all three life history phases and of unknown life history phase, there was a trend of higher percentage breakage in larger size classes. For female gametophyte thalli (Fig. 4A), percentage breakage was 19.9±5.7% (mean±95% confidence interval, N=22) for the smallest size class (0–10 cm), 33.5±8.1% (N=21) for the medium size class (10–20 cm) and 67.7±15.5% (N=10) for the largest size class (20–35 cm). For tetrasporophyte thalli (Fig. 4B), percentage breakage was 21.6±4.2% (N=22) for the smallest size class, 36.0±9.2% (N=22) for the medium size class and 43.4±28.6% (N=7) for the largest size class. For male gametophyte thalli (Fig. 4C), percentage breakage was 19.9±7.5% (N=22) for the smallest size class, 39.1±8.9% (N=21) for the medium size class and 59.6±19.2% (N=9) for the largest size class. For thalli of unknown life history phase (Fig. 4D), percentage breakage was 24.8±6.7% (N=22) for the smallest size class and 60.2±18.5% (N=9) for the medium size class; no longest fronds were ever in the largest size class.

The trend of higher percentage breakage in larger size classes was assessed with statistical tests. For female gametophyte thalli

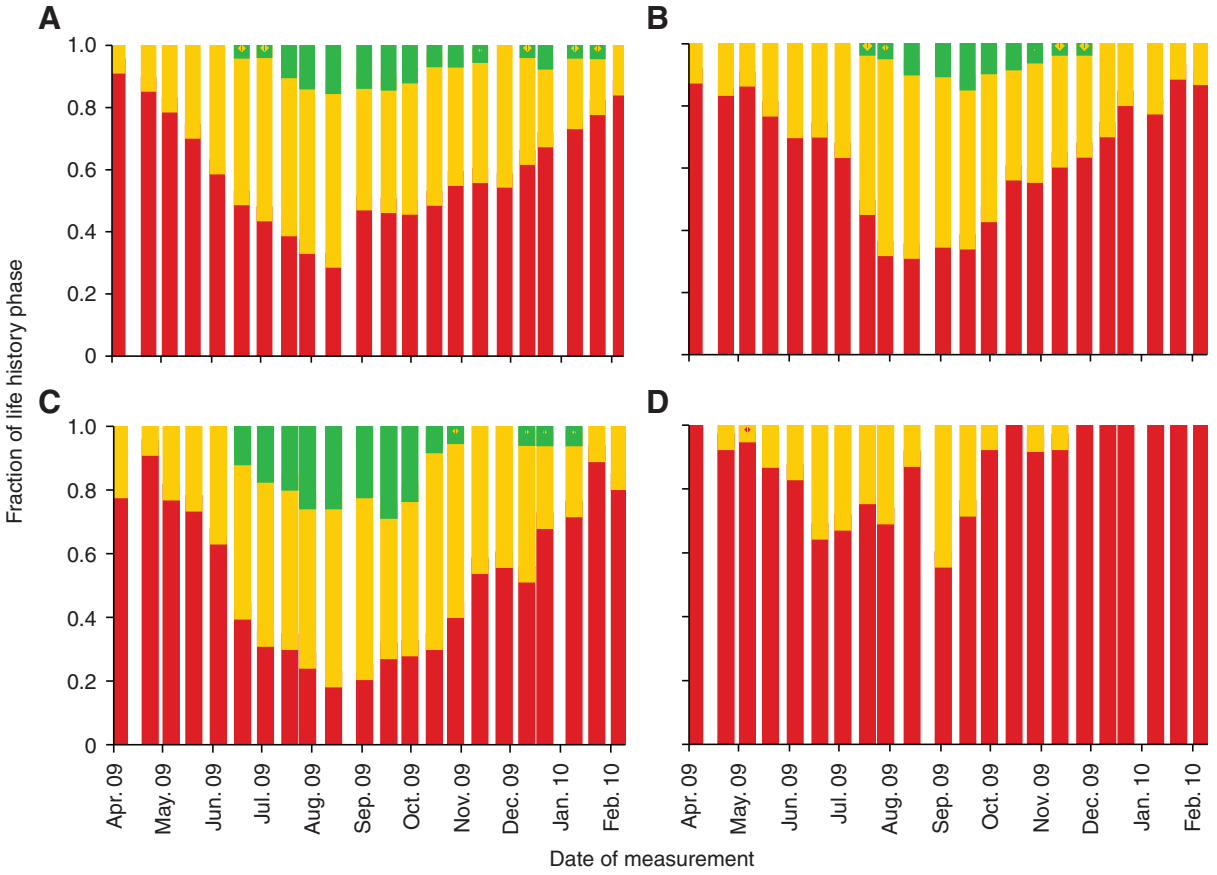

Fig. 1. For every tidal cycle from April 2009 to February 2010: fraction of longest *M. flaccida* fronds in three size classes for tagged female gametophyte thalli (A), tetrasporophyte thalli (B), male gametophyte thalli (C) and thalli of unknown life history phase (D). Size classes are as follows: length of 0–10 cm (red bottom-most bars), 10–20 cm (yellow bars in middle) and 20–35 cm (green uppermost bars).

(Fig. 4A), percentage breakage of longest fronds was significantly greater for the largest size class than for the medium size class, which in turn displayed significantly more breakage than the smallest size class (ANOVA, $F_{2,50}$=27.95, P<0.0001; variances homogeneous: Brown–Forsythe test, P=0.27; Tukey HSD). Similarly, for male gametophyte thalli (Fig. 4C), percentage breakage of longest fronds was significantly greater for the largest size class than for the medium size class, which in turn experienced significantly more breakage than the smallest size class (ANOVA, $F_{2,49}$=14.09, P<0.0001; variances homogeneous: Brown–Forsythe test, P=0.37; Tukey HSD). Also, for thalli of unknown life history phase (Fig. 4D), percentage breakage of longest fronds was greater for the medium size class than for the smallest size class [two-tail t-test, unequal variances (Ruxton, 2006), t=–4.09, P=0.002]. For tetrasporophyte thalli (Fig. 4B), there was a significant trend of higher percentage breakage for the largest and medium size classes compared with the smallest size class (ANOVA, $F_{2,48}$=5.15, P=0.009; variances heterogeneous: Brown–Forsythe test, P=0.002; Tukey HSD; Kruskal–Wallis test, P=0.028).

Measurements for fatigue-breakage model

Frond area relevant to drag

For the drag-force equation used in the fatigue-breakage model (Eqn 3), single-sided frond surface area A was determined as a function of the product of frond length L (cm) and frond maximal width W (cm) and plotted on logarithmic axes (Fig. 5). Life history phase did not affect the relationship between logLW and log$A$: linear regressions for fronds of the three life history phases and of unknown life history phase had indistinguishable slopes and demonstrated no effect of life history phase (ANCOVA: life history phase×logLW, $F_{3,220}$=0.83, P=0.48; life history phase, $F_{3,220}$=0.80, P=0.49). Accordingly, all logarithmic data for A and the product of L and W were fitted with a single regression equation: log$A$=0.9958log(LW)–0.2219, R^2=0.99, P≪0.001, with A in this equation in cm^2. Standard deviation of the residuals was 0.075log cm^2. A was converted to m^2 for use in the model.

Mazzaella flaccida drag coefficients

From previously collected u *versus* C_D data for *M. flaccida* fronds (Mach, 2009), the standard deviation of residuals, sd$_R$, was determined as a function of u for u≤9.5 m s^{-1}: sd$_R$=0.024$u^{-3.071}$, R^2=0.99.

Fatigue behavior

Mazzaella flaccida 1 Hz fatigue data without pauses (Mach 2009) and with pauses are given in Fig. 6. Linear regressions for these data had indistinguishable slopes and revealed no effect of loading pauses (ANCOVA: pause treatment×logN_{br}, $F_{1,186}$=0.08, P=0.77; pause treatment, $F_{1,186}$=0.01, P=0.91). Likewise, when each life history phase was analyzed separately, linear regressions had indistinguishable slopes with no effects of loading pauses (ANCOVA for female gametophytes: pause treatment×logN_{br}, $F_{1,58}$=3.22, P=0.08; pause treatment, $F_{1,58}$=1.37, P=0.25; ANCOVA for tetrasporophytes: pause treatment×logN_{br}, $F_{1,60}$=0.002, P=0.97; pause treatment, $F_{1,60}$=0.49, P=0.49; ANCOVA for male

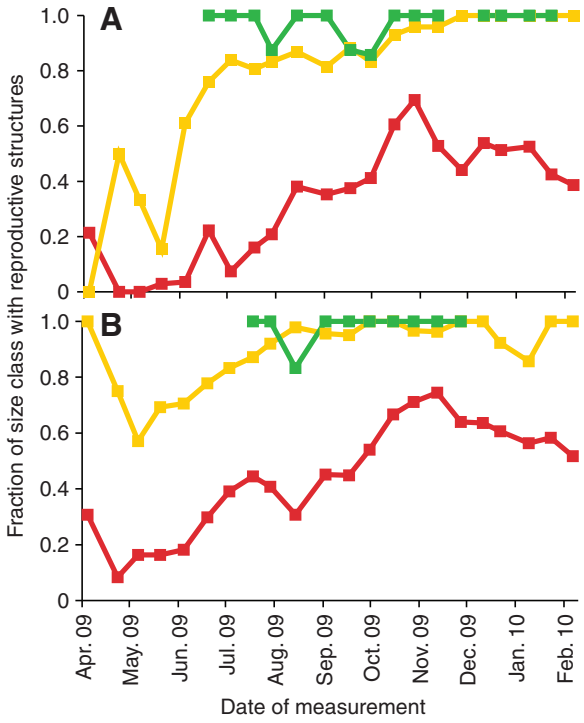

Fig. 2. For tidal cycles from April 2009 to February 2010: the fraction of longest *M. flaccida* fronds in each size class exhibiting reproductive structures for tagged female gametophyte thalli (A) and tetrasporophyte thalli (B). Size classes are as follows: length of 0–10 cm (in red), 10–20 cm (in yellow) and 20–35 cm (in green).

gametophytes: pause treatment×logN_{br}, $F_{1,60}$=0.10, P=0.75; pause treatment, $F_{1,60}$=0.000, P=0.99).

Pull-to-break strengths

For field tests of *M. flaccida*, breaking forces were found for all life history phases and for *M. flaccida* overall: 8.75±3.07 N for female gametophytes (mean ± s.d.), 9.33±3.32 N for tetrasporophytes, 10.14±3.72 N for male gametophytes and 9.41±3.41 N for *M. flaccida* overall. Pull-to-break strengths were also determined: 3.25±2.80 MPa for female gametophytes (mean ± s.d.), 2.34±1.79 MPa for tetrasporophytes, 3.30±3.20 MPa for male gametophytes and 2.96±2.68 MPa for *M. flaccida* overall. For 150 tested fronds, break locations were as follows: 9 (6%) in the blade, 19 (12.7%) in the stipe, 75 (50%) in the stipe–holdfast junction, 15 (10%) in the holdfast and 32 (21.3%) in the substratum.

Breaking force measured in the field did not vary with life history phase (ANOVA, $F_{2,147}$=2.14, P=0.12; variances homogeneous: Brown–Forsythe test, P=0.36). Breaking stress also did not vary with life history phase (ANOVA on log-transformed data, $F_{2,147}$=0.46, P=0.63; variances homogeneous: Brown–Forsythe test, P=0.37).

Maximal wave-induced velocities

For all 10 study sites, the relationship between offshore significant wave height H_S and maximal onshore wave-induced water velocity u_{max} was better fitted by an asymptotic (Eqn 1) rather than linear (Eqn 2) regression, as evidenced by the higher R^2 for the asymptotic regression in all cases. Asymptotic regression equations are given in Table 2, and data from two representative sites are shown in Fig. 7.

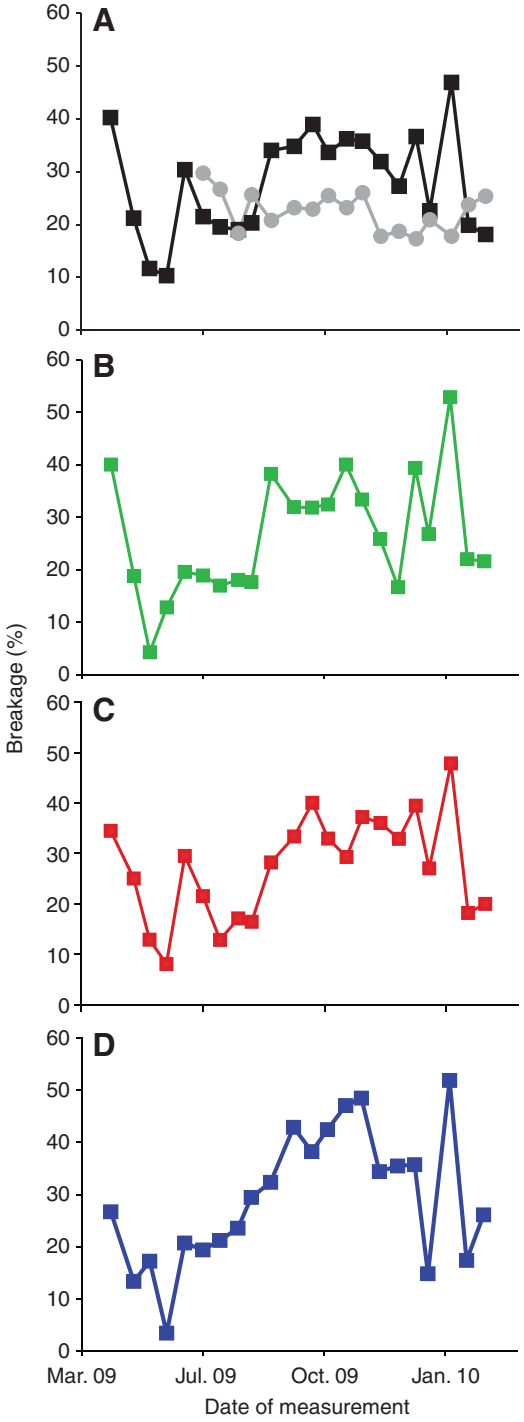

Fig. 3. For every tidal cycle from April 2009 to February 2010: the percentage breakage for longest fronds in tagged *M. flaccida* thalli, for all fronds (A, black squares), female gametophytes (B), tetrasporophytes (C) and male gametophytes (D). Breakage was defined as the longest frond in a thallus decreasing in length by 1 cm or more between measurements. In A, maximal temperature (°C) during each tidal-cycle deployment at each site, averaged across all sites, is also shown (gray circles).

Non-maximal wave-induced velocities

Cumulative probability distributions of normalized peak wave-induced velocities $u_{p,norm}$ are shown for 399 days of continually recorded wave data in Fig. 8A. The mean cumulative probability distribution, as computed over 100 bins of normalized velocity, is

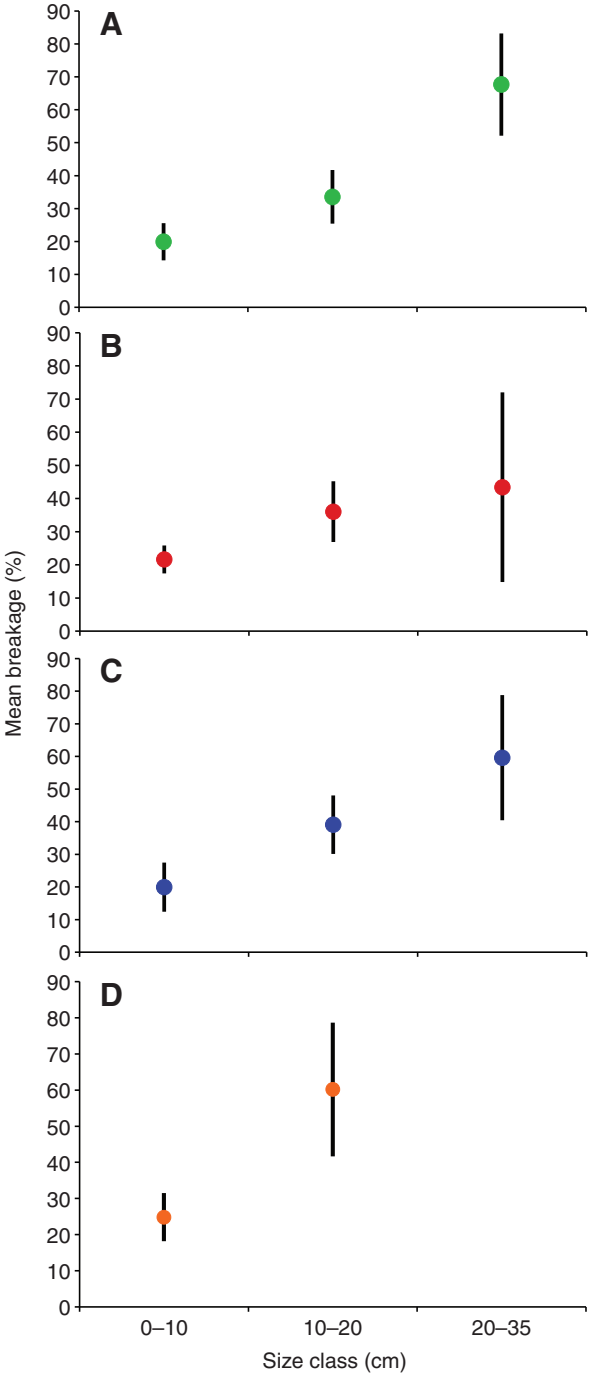

Fig. 4. Mean percentage breakage ±95% confidence interval for each size class of longest fronds in tagged female gametophyte thalli (A), tetrasporophyte thalli (B), male gametophyte thalli (C) and thalli of unknown life history phase (D). Means were taken over tidal-cycle measurements for which 2 or more thalli were present in the category.

depicted in Fig. 8B along with a fitted 6th-order polynomial. An approximate probability density function, determined from the slope of the mean cumulative probability distribution, is given in Fig. 8C. A frequency histogram of all collected $u_{p,norm}$ is shown in Fig. 8D.

Breakage predictions

Breakage predictions for thalli of each life history phase and also of unknown life history phase are depicted in Fig. 9. Predictions are

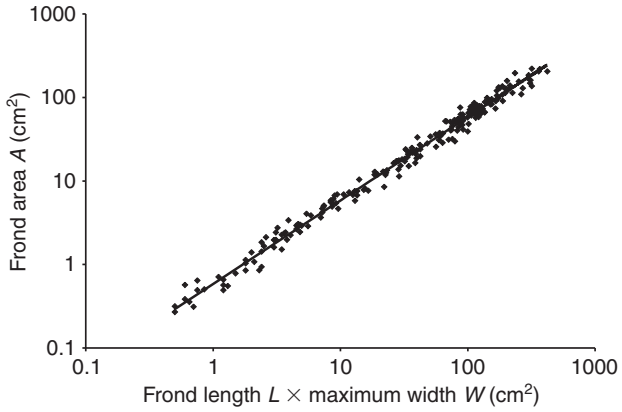

Fig. 5. On logarithmic axes, single-sided frond surface area A (here given as cm^2) is shown as a function of the product of frond length L (cm) and frond maximal width W (cm) for all measured fronds. The black line is the best-fit regression line.

given as the ratio of the number of fronds predicted to break to the number of fronds actually measured as breaking in field surveys. For each life history phase category, ratios were averaged over all tidal-cycle measurements. Ratios for the fatigue-breakage model, which included breakage predicted from individual as well as repeated wave-induced forces, were as follows: 1.05±0.21 (mean ratio ±95% confidence interval) for female gametophytes, 0.79±0.18 for tetrasporophytes, 0.51±0.14 for male gametophytes and 0.26±0.12 for unknown life history phase. Ratios only including failure due to maximal individual wave-induced force (‘traditional model’) were as follows: 0.57±0.15 (mean ratio ±95% confidence interval) for female gametophytes, 0.57±0.11 for tetrasporophytes, 0.30±0.13 for male gametophytes and 0.15±0.09 for unknown life history phase. Ratios varied with life history phase category and with prediction method (fatigue-breakage or traditional model) (two-

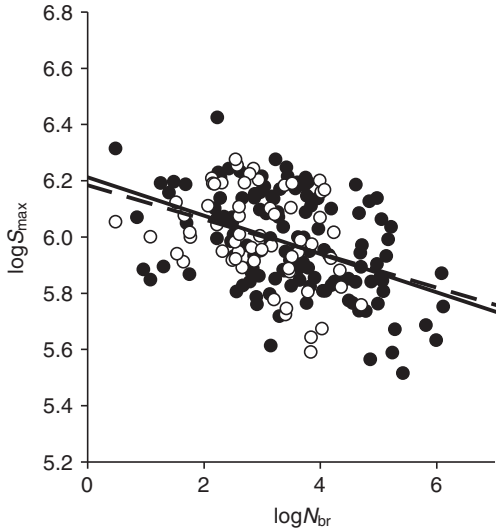

Fig. 6. Fatigue data for *M. flaccida* tested at 1 Hz, without and with pauses (without pauses, black circles; with pauses, white circles). Without pauses, fatigue-test loadings were continuous; with pauses, there were 9 s between loadings. Linear regression equations are as follows: without pauses (solid line), $\log S_{max}=-0.0681\log N_{br}+6.2120$, $R^2=0.20$, $P\ll0.001$; with pauses (dashed line), $\log S_{max}=-0.0607\log N_{br}+6.1845$, $R^2=0.11$, $P=0.008$. N_{br}, number of cycles to breakage.

Table 2. Regressions for maximal wave-induced velocities at *M. flaccida* study sites

Site	u_{asym}	H_K	R^2	P	N	s.d. of residuals (m s^{-1})
1	16.290	1.050	0.13	<0.01	101	4.745
2	16.260	1.755	0.48	<0.001	71	2.580
3	20.630	1.812	0.47	<0.001	71	3.111
4	15.151	1.866	0.29	<0.05	79	3.315
5	23.953	1.124	0.23	<0.001	140	6.443
6	17.767	0.874	0.22	<0.01	69	5.258
7	47.119	3.262	0.41	<0.05	136	6.308
8	22.632	0.976	0.19	<0.01	84	6.489
9	13.380	0.615	0.16	<0.0001	86	3.255
10	13.622	0.883	0.25	<0.001	70	3.520

Regression equation: $u_{max}=u_{asym}[1-\exp(-H_S/H_K)]$; where u_{max} is maximal onshore wave-induced velocity (m s^{-1}), H_S is offshore significant wave height (m) and u_{asym} and H_K are fitted constants.
See also Fig. 7.

way ANOVA, life history phase, $F_{3,126}$=29.07, P<0.0001; prediction method, $F_{1,126}$=26.12, P<0.0001; variances homogeneous: Brown–Forsythe test, P=0.48). Ratios were significantly higher for female gametophytes and tetrasporophytes than for male gametophytes, for which ratios were significantly higher than for thalli of unknown life history phase; additionally, ratios were significantly greater for the fatigue-breakage model than for the traditional model (Tukey HSD).

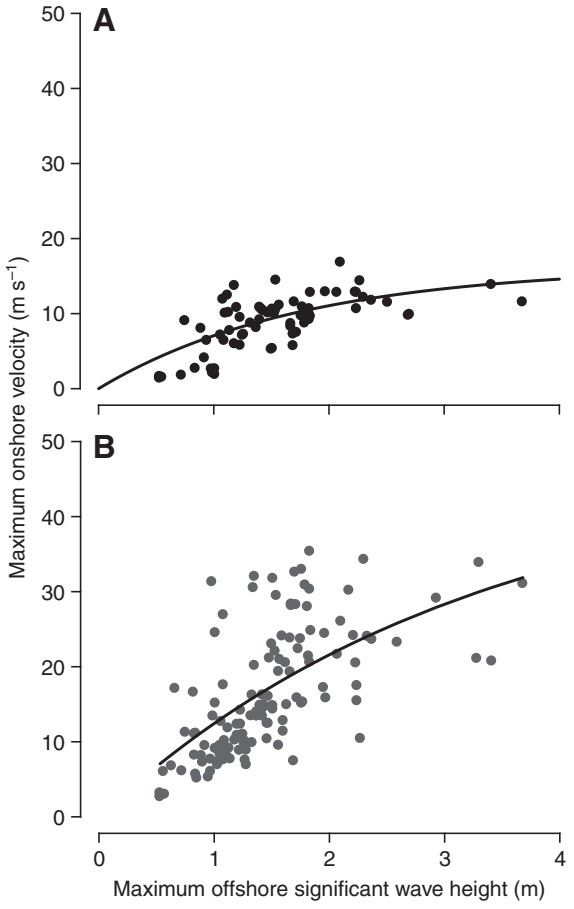

Fig. 7. Maximal onshore wave-induced velocity u_{max} (m s^{-1}) as a function of maximal offshore significant wave height H_S (m) for 2 of the 10 study sites. (A) Data and asymptotic regression for site 2, a site with relatively low wave-induced velocities. (B) Data and asymptotic regression for site 7, a site with relatively high wave-induced velocities. Regression equations are given in Table 2.

Predicted-to-actual ratios, averaged over all tidal-cycle measurements for female gametophytes, tetrasporophytes and male gametophytes, were assessed for categories of quantified attributes. For both fatigue-breakage and traditional models, ratios were significantly higher for unbleached fronds than for fronds displaying bleaching [Fig. 10A; fatigue-breakage model: two-tail t-test, unequal variances (Ruxton, 2006), t=3.28, P=0.002; traditional model: two-tail t-test, unequal variances, t=2.84, P=0.007]. In other words, fronds with bleaching experienced more field-observed breakage than predicted by the models, reducing the ratios of predicted-to-actual breakage. Ratios were significantly lower for fronds with endophytes than for fronds lacking endophytes for the traditional model but not significantly so for the fatigue-breakage model (Fig. 10B; fatigue-breakage model: two-tail t-test, unequal variances, t=1.20, P=0.23; traditional model: two-tail t-test, unequal variances, t=2.07, P=0.04). A similar result (not depicted graphically) was found if attribute numbers for endophytes and for epiphytes, which were relatively rare over the course of the study, were combined: for the traditional model, ratios were significantly higher for fronds without endophytes and epiphytes, and for the fatigue-breakage model, ratios were higher, but not significantly so, for fronds without endophytes or epiphytes (fatigue-breakage model: two-tail t-test, unequal variances, t=1.18, P=0.24; traditional model: two-tail t-test, unequal variances, t=2.22, P=0.03). For the fatigue-breakage model but not for the traditional model, ratios were significantly lower in the most holey and tattered category of fronds (attribute sum of 4–9) as compared with the moderate holey and tattered category (attribute sum of 2–3) (Fig. 10C; fatigue-breakage model: ANOVA, holes and tattering, $F_{2,139}$=3.51, P=0.03; variances homogeneous: Brown–Forsythe test, P=0.08; Tukey HSD; traditional model: ANOVA, holes and tattering, $F_{2,139}$=1.48, P=0.23; variances homogeneous: Brown–Forsythe test, P=0.23). Ratios were also evaluated for the sum of many attributes: holes, tattering, bleaching, herbivore markings, endophytes and epiphytes (Fig. 10D). Ratios did not vary with attribute sum for the traditional model (Kruskal–Wallis test, P=0.083), but ratios varied with attribute sum for the fatigue-breakage model: ratios were significantly higher for the lowest attribute-sum category (0–1) than for the higher attribute-sum categories (4–5 and 6–25), which in turn had significantly different ratios (Kruskal–Wallis test, P=0.007; Tukey HSD). Ratios did not vary with reproductive number over four categories (0, 1–2, 3–4 and 5) for either the fatigue-breakage model or the traditional model (not depicted graphically; fatigue-breakage model: ANOVA, reproductive number, $F_{3,123}$=1.47, P=0.23; variances homogeneous: Brown-Forsythe test, P=0.25; traditional

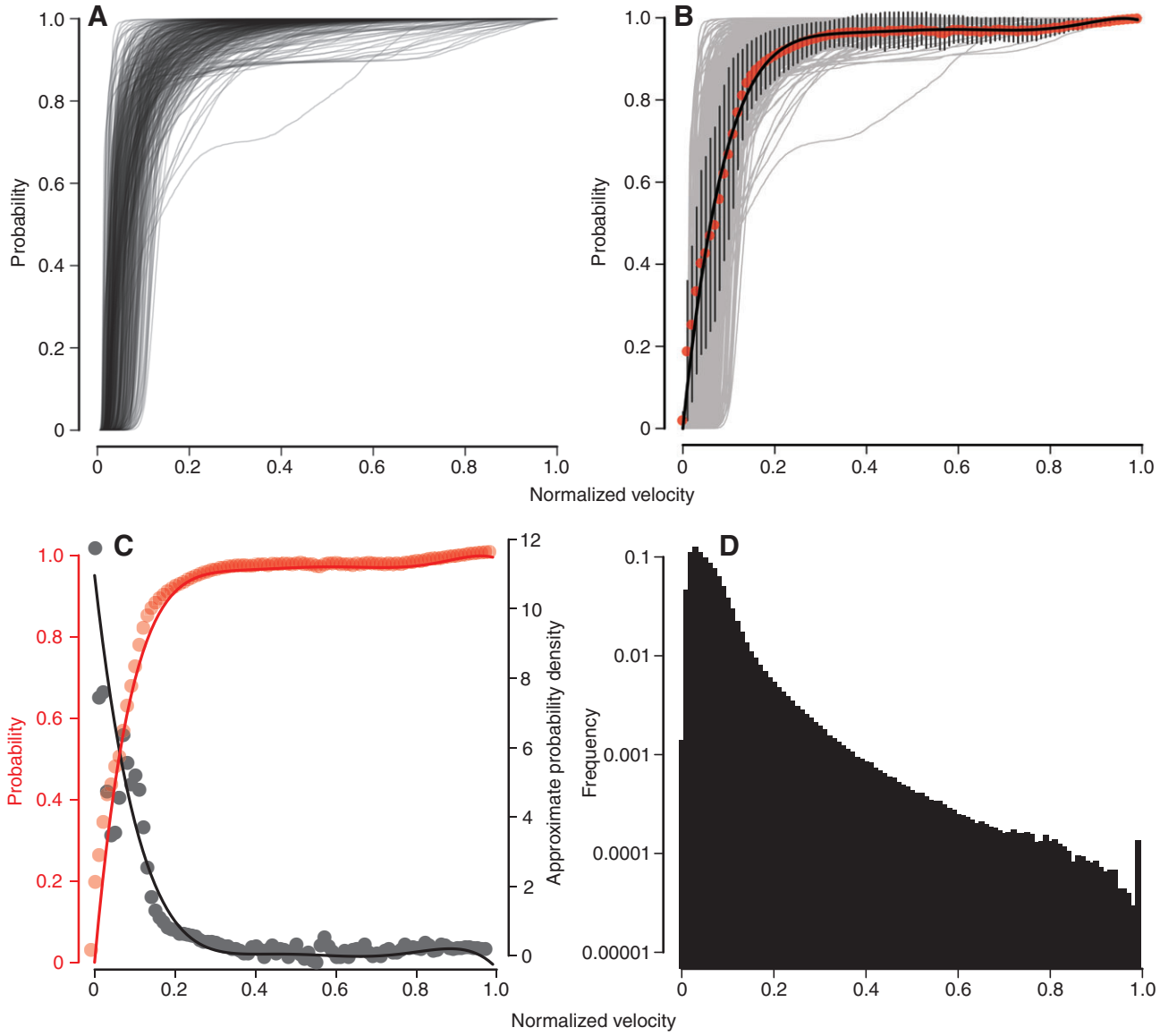

Fig. 8. (A) Cumulative probability distributions of normalized peak wave-induced velocities $u_{p,norm}$ for 399 days of continually recorded wave data. Each line depicts the cumulative probability distribution for 1 day of data. (B) Mean probability for all cumulative probability distributions (red circles), with standard deviations (black vertical bars), for 100 bins of normalized velocity. Cumulative probability distributions are given in the background (gray lines). A 6th-order polynomial was fitted to the mean cumulative probability distribution: probability=$-32.1435u_{p,norm}^{6}+115.6497u_{p,norm}^{5}-167.5870u_{p,norm}^{4}+125.4108u_{p,norm}^{3}-51.2982u_{p,norm}^{2}+10.9603\ u_{p,norm}$, R^2=0.99, P<0.001 (curved black line). (C) Mean cumulative probability distribution (red circles) along with the 6th-order fitted polynomial (red curved line). A probability density function was estimated from the slope of the mean cumulative probability distribution (gray circles and black curved line). (D) A frequency histogram of all $u_{p,norm}$ (N=3,447,360) for 100 bins of normalized velocity, with the ordinate axis logarithmic.

model: ANOVA, reproductive number, $F_{3,123}$=2.01, P=0.12; variances homogeneous: Brown–Forsythe test, P=0.054).

Predicted-to-actual ratios varied with an index of logger exposure for the fatigue-breakage and traditional models (Fig. 11A). Site velocity exposure index (m s^{-1}) was taken as the mean velocity predicted at a site for H_S=3.5 m, from regression equations given in Table 2. Other attributes of fronds were also assessed across logger exposures. Only frond area A and holes-and-tattering attribute sum were found to vary with logger exposure (Fig. 11B,C). For the three life history phases, linear regressions fitted to frond area A as a function of logger exposure index had indistinguishable slopes and demonstrated a significant effect of life history phase; A was significantly greater for male gametophytes than for tetrasporophytes (ANCOVA: life history phase×index, $F_{2,24}$=0.31, P=0.74; life history phase, $F_{2,24}$=7.01, P=0.004, Tukey HSD; index, $F_{1,24}$=6.74, P=0.016). The sum of holes and tattering number varied significantly with velocity exposure index but not with life history phase (ANCOVA: life history phase×index, $F_{2,24}$=1.13, P=0.34; life history phase, $F_{2,24}$=3.46, P=0.048, Tukey HSD; index, $F_{1,24}$=18.62, P=0.0002). Regressions fitted to bleaching number, endophyte number and reproductive number across logger exposure indices were not significant (P>0.05).

DISCUSSION

Comparison of observed breakage trends to prior predictions from laboratory fatigue testing

Extending laboratory assessments of fatigue breakage, Mach (Mach, 2009) translated stresses imposed on *M. flaccida* specimens

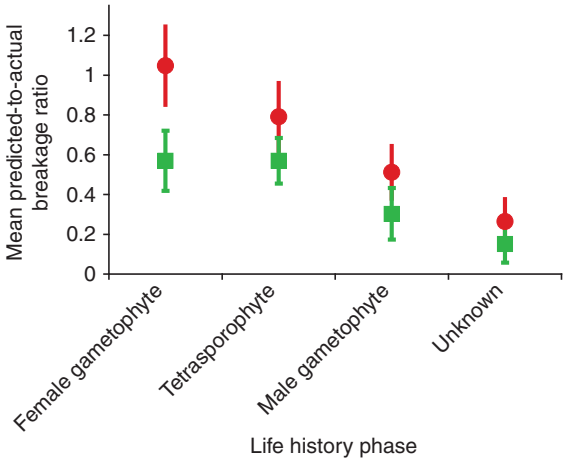

Fig. 9. For all tidal cycles, mean ratio ±95% confidence interval of predicted-to-actual breakage for thalli of all three life history phases and also for thalli of unknown life history phase. Ratio was averaged over all tidal-cycle measurements. Predictions from the fatigue-breakage model (red) include breakage due to individual and repeated wave-induced forces. Predictions as traditionally made (green) only include breakage due to the largest individual wave-induced force in each period of measurement. A ratio of 1 would indicate that the model predicts all breakage due to wave-imposed forces and that all breakage in the field is due to wave-imposed forces. The fatigue-breakage model accounted for significantly more breakage than the traditional method. Additionally, the predicted-to-actual breakage ratio varied with life history phase, being significantly greater for female gametophytes and tetrasporophytes.

in the laboratory to equivalent wave-imposed water velocities that would induce those stresses in fronds in the field [fig. 12 in Mach (Mach, 2009)]. These translations yielded two predictions about field breakage. First, larger fronds were predicted to break by fatigue more frequently than smaller fronds. Second, fatigue failure of *M. flaccida* blades was predicted to vary with life history phase; female gametophyte fronds were predicted to be most susceptible to breakage by fatigue, and male gametophyte fronds least susceptible, with tetrasporophyte fronds displaying intermediate susceptibility.

For the present study, the question then arises: were observed trends in field breakage of *M. flaccida* fronds consistent with prior predictions for frond size and life history phase? Data depicted in Fig. 4 indicate that breakage varied as expected with frond size. For fronds of all life history phases, as well as unknown life history phase, percentage breakage observed during tidal-cycle measurements increased with increasing frond size. Observed breakage trends were thus consistent with the prior prediction that susceptibility to breakage by fatigue increases with increasing frond size.

However, data in Fig. 4 do not obviously support the prediction of greatest susceptibility to fatigue breakage in female gametophyte fronds and of least susceptibility in male gametophyte fronds. Indeed, mean percentage breakage for each of the three size classes was similar across the three life history phases and did not show consistent trends of greatest breakage for female gametophytes and least breakage for male gametophytes. Along related lines, previous research on *M. splendens* (Setchell and Gardner) Fredericq determined that gametophyte and sporophyte fronds display similar survivorship (May, 1986; Dyck and DeWreede, 2006a).

Another possible manifestation of different susceptibility to fatigue breakage across life history phases is greater limitation of frond area *A* in fronds most susceptible to fatigue breakage, an

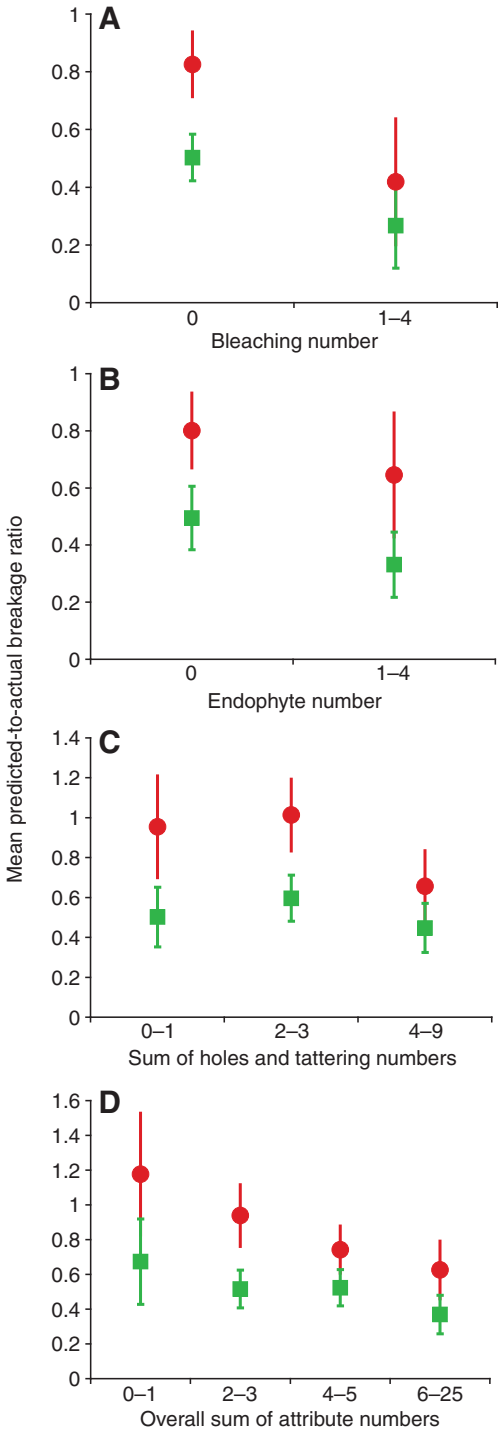

Fig. 10. Mean ratio ±95% confidence interval of predicted-to-actual breakage as a function of various quantified attributes for fatigue-breakage model (red) and traditional maximal-force model (green). The ratio was averaged over all tidal-cycle measurements for female gametophyte, tetrasporophyte and male gametophyte thalli. (A) For the fatigue-breakage model and the traditional method, significantly more breakage was accounted for in unbleached blades. (B) For the traditional model, significantly more breakage was accounted for in the absence of endophytes. (C) For the fatigue-breakage model, significantly more breakage was accounted for in fronds with fewer holes and less tattering. (D) Attributes summed for this plot included numbers for bleaching, tattering, holes, herbivore markings, endophytes and epiphytes. For the fatigue-breakage model, significantly more breakage was accounted for at lower overall attribute sums.

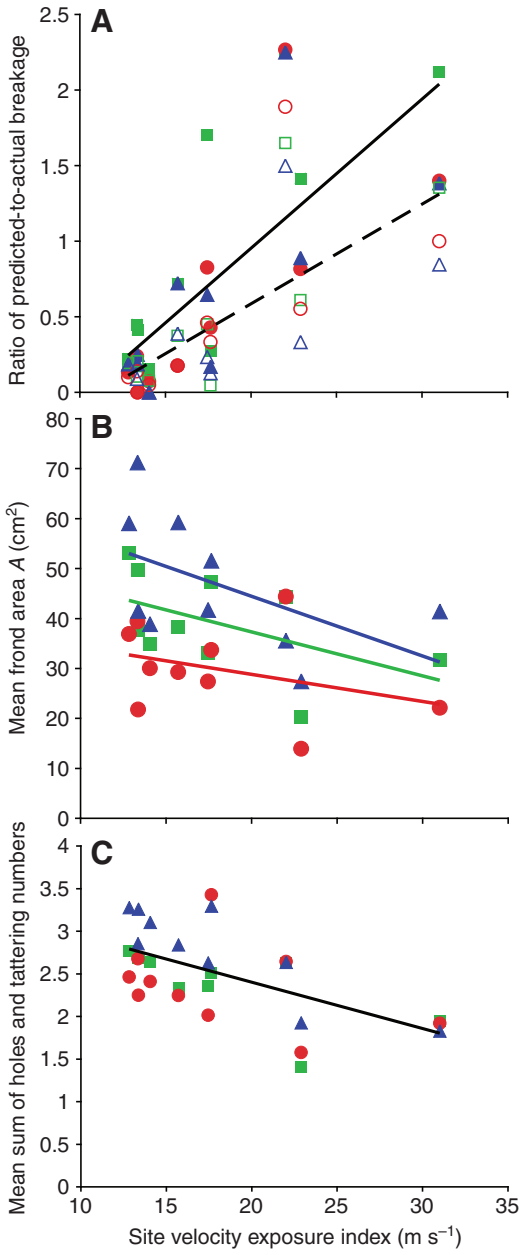

Fig. 11. (A) Ratio of predicted-to-actual breakage for the fatigue-breakage model (solid symbols) and for the traditional maximal-force model (open symbols) as a function of site velocity exposure index (m s^{-1}). For each site, velocity exposure index is velocity predicted at the site for H_S=3.5 m through the appropriate regression equation (e.g. Fig. 7, Table 2). Overall breakage ratio at each site is given for tagged tetrasporophyte thalli (red), female gametophyte thalli (green) and male gametophyte thalli (blue). Linear regression equations are as follows: for fatigue-breakage model (solid line), ratio=0.0986index–1.0196, R^2=0.55, P<0.0001; for traditional maximal-force method (dashed line), ratio=0.0659index–0.7326, R^2=0.50, P<0.0001. (B) Mean single-sided frond surface area A (here given as cm^2) as a function of site velocity exposure index for longest fronds of tagged tetrasporophyte thalli (red), female gametophyte thalli (green) and male gametophyte thalli (blue). A varied with velocity exposure index and with life history phase. (C) Mean sum of holes and tattering numbers as a function of site velocity exposure index for longest fronds of tagged tetrasporophyte thalli (red), female gametophyte thalli (green) and male gametophyte thalli (blue). A sum of 0 indicates no holes or tattering, while a sum of 9 indicates complete frond coverage by holes and tattering. Linear regression equation for all life history phases combined is sum=–0.0544index+3.4908, R^2=0.36, P<0.001 (black line).

outcome that would reduce wave-imposed force as described by Eqn 3. This possibility can be assessed to some extent with data presented in Fig. 11B. For all three life history phases, frond area decreased with increasing wave exposure of sites. In addition, frond area was significantly smaller for tetrasporophytes than for male gametophytes, consistent with prior predictions from laboratory results. But contrary to prior predictions, female gametophytes displayed intermediate frond area not significantly different from male gametophyte or tetrasporophyte frond size (Fig. 11B). Previous studies of *M. splendens* similarly found tetrasporophytes to have smaller frond area than gametophytes (May, 1986; Shaughnessy et al., 1996). In sum, field breakage may to some degree show consistency with the prediction of fatigue-breakage susceptibility varying with life history phase. Consistent trends, though, were demonstrated through frond-area data for male gametophytes and tetrasporophytes, not through overall breakage rates for the life history phases.

Loadings in the laboratory *versus* the field

Quantified fatigue behavior of *M. flaccida*, as documented in Mach (Mach, 2009) and then employed in this study, involved fatigue loadings that were stress controlled, tensile and sinusoidal in profile, with minimum stress always of 0 Pa and frequency of 1 Hz. Loadings were consistent with standard engineering testing techniques but prompt the question: can these loadings be compared with loadings due to breaking waves in the field?

In the field, *M. flaccida* experiences a wave every 9–10 s, with substantial velocities occurring over fractions of seconds to several seconds during each wave. As in the field, laboratory loadings had minimum stress of 0 Pa, equivalent to periods of no loading between waves. Nonetheless, loadings exerted on *M. flaccida* fronds by breaking waves differ from imposed laboratory loadings in two substantial ways. First, each loading cycle in the laboratory lasted for 1 s. In contrast, durations of wave-imposed field loadings vary. Second, while loadings in the laboratory were continuous, with each loading immediately followed by the next, loadings in the field are punctuated with periods of no loading between waves. To directly compare loadings in the laboratory and field, we first needed to assess effects on fatigue behavior of loading frequency and of pauses between loadings.

Mach (Mach, 2009) evaluated effects of loading frequency on fatigue behavior, testing specimens at 0.5, 1 and 2 Hz to span typical loading frequencies in the field. Mach (Mach, 2009) determined that there was a marginal effect of loading frequency but, overall, loading frequency demonstrated a relatively small effect on fatigue behavior in contrast to frond attributes such as life history phase. Then, in the present study, we found that pauses of 9 s between loadings, mimicking periods of no loading between waves, did not alter fatigue behavior (Fig. 6).

In summary, *M. flaccida* fatigue behavior did not vary substantially with either loading frequency or loading pauses. As a result, fatigue behavior determined with continual 1 Hz loadings in the laboratory can likely be used to evaluate fatigue damage due to wave-associated loadings in the field. Additional research might assess whether other characteristics of wave-induced loadings, such as non-sinusoidal waveforms and effects of frond flapping, limit the degree to which fatigue damage due to these loadings can be approximated through fatigue behavior measured with sinusoidal loadings imposed in the laboratory.

Locations of breakage

Breakage model predictions in this study evaluated breakage in *M. flaccida* blades. Breakage can occur in other locations in *M. flaccida* thalli: in the stipes, stipe–holdfast junctions, holdfasts and substratum. Nonetheless, for *M. flaccida*, the exact distribution of breakage locations in thalli exposed to breaking waves remains unknown. This study's measurements of *M. flaccida* breakage in the field could not distinguish breakage locations because entire thalli were tracked, each with multiple fronds not individually marked. Initial investigations of *Mazzaella* strength in the field, as corroborated by field tests of *M. flaccida* strength in this study, found that breakage occurred primarily at stipe-holdfast junctions when fronds were folded, clamped and pulled parallel to the substratum. (Shaughnessy et al., 1996). We found, for example, that 50% of breakage occurred at the stipe–holdfast junction when testing frond strength with this method. However, measurements of wave-induced (not researcher-induced) breakage contradicted initial results, finding that fracture occurred more often in blades than at stipe–holdfast junctions (Shaughnessy and DeWreede, 2001). Thus, model predictions in this study assessed breakage where it often occurs, in frond blades, although other breakage locations are possible in *M. flaccida* fronds and thalli.

The importance of fatigue for natural populations of *M. flaccida*

Traditional biomechanical methods of predicting macroalgal breakage due to wave-imposed forces generally have underestimated, and often greatly underestimated, breakage rates. By developing and testing a fatigue-breakage model in this study, we can conclude that repeated wave forces, not just individual maximal forces, very likely break intertidal seaweeds through the process of fatigue.

The fatigue-breakage model we created predicted significantly more breakage for *M. flaccida* than did traditional prediction methods, and these fatigue-based predictions are closer to reality (Fig. 9). Whereas traditional breakage models only consider breakage due to the largest individual wave-induced forces, the fatigue-breakage model used here also included breakage due to repeated, sub-maximal wave-induced forces. For *M. flaccida*'s three life history phases as well as for *M. flaccida* of unknown life history phase, nearly twice as much breakage observed in the field was accounted for by considering effects of repeated wave-induced loadings through the fatigue-breakage model (Fig. 9).

The metric used to assess model performance, the ratio of predicted-to-actual breakage, would have a value of 1 if the model accurately predicted all breakage due to waves and if all field breakage were actually due to wave-imposed forces. For the two life history phases for which the fatigue-breakage model accounted for the most breakage (Fig. 9), female gametophytes and tetrasporophytes, ratios of predicted-to-actual breakage assumed mean values of 1.05 and 0.79, respectively, indicating that fatigue breakage as modeled may explain most breakage in the field for these life history phases. The mean ratio for male gametophytes was lower, 0.51, suggesting that male gametophyte fronds break more often than expected on the basis of their fatigue behavior and resulting fatigue damage. Fronds of unknown life history stage had the lowest ratio of predicted-to-actual breakage for the fatigue model, 0.26, perhaps because frond properties were poorly approximated using overall *M. flaccida* mean.

It was initially hypothesized that various *M. flaccida* frond attributes, such as the presence of bleached tissue, endophytes, or holes and tattering, might cause the model to under-predict breakage – that is, cause the ratio of predicted-to-actual breakage to fall below 1. Evaluation of breakage-model ratios did demonstrate trends, some significant, as expected for several attributes: bleaching, which is indicative of temperature stress; endophytes; holes and tattering; and an overall attribute sum. In finding that several frond characteristics (most notably, bleaching, large amounts of holes and tattering, and large overall attribute sums) significantly decreased the ratio of predicted-to-actual breakage, we can conclude that frond characteristics may weaken fronds and increase the likelihood of breakage, over rates predicted on the basis of material properties. Endophytes in macroalgal fronds have been reported to diminish frond growth rates, reproductive output and survivorship (Correa et al., 1994; Buschmann et al., 1997; Faugeron et al., 2000; Apt, 2004), and the results of this study suggest along similar lines that endophyte presence increased frond breakage rates. Even though reproductive structures were previously determined to reduce fatigue strength (Mach, 2009), ratios did not vary with the presence of reproductive tissues, a result consistent with Dyck and DeWreede's observation of no change in survival probability following the onset of reproduction for *M. splendens* (Dyck and DeWreede, 2006a).

Ultimately, wave exposure of sites may have influenced model predictions most. Ratios of predicted-to-actual breakage fell below 1 at the most wave-protected sites and exceeded 1 at the most wave-exposed sites (Fig. 11A). This outcome may suggest that, at the most protected sites, fronds are more likely to break from physiological stressors besides fatigue damage. At the most exposed sites, fronds are perhaps more able to resist fatigue breakage than typical fronds in the population, potentially possessing greater strength. Another red macroalga, *Mastocarpus papillatus* (C. Agardh) Kützing, similarly displayed a greater ability to resist breakage along a gradient of increasing exposure to wave-induced forces (Kitzes and Denny, 2005).

Because *M. flaccida* consists of living tissue, biological repair may remedy some damage due to fatigue. Fronds tested in the laboratory to establish fatigue behavior were collected throughout the year, and season did not influence measured fatigue properties (Mach, 2009). Therefore, *M. flaccida* likely does not alter its fatigue properties in response to wave climate, which shifts over the course of the year. Laboratory tests of individual specimens lasted in some cases up to 2 weeks, the approximate tidal-cycle prediction period assessed in this study. In these respects, *M. flaccida*'s documented fatigue behavior can be expected to reflect fatigue properties of *M. flaccida* fronds in the field throughout the year. Nonetheless, some potentially relevant scenarios were not tested. For example, if a frond sustains fatigue damage, such as a small crack, during a series of large waves but then repairs the damage in a subsequent period of calm wave conditions, sustained fatigue damage may no longer contribute to failure as predicted by the fatigue-breakage model. Such scenarios of biological repair could be fruitfully assessed in subsequent studies.

Overall, this study takes several substantial steps forward in understanding breakage of macroalgal fronds as actually occurs in the field. Whereas wave-imposed velocities experienced by *M. flaccida* were previously poorly understood (Mach, 2009), this study robustly quantifies both maximal and sub-maximal wave-associated velocities relevant to *M. flaccida* and other intertidal organisms (Figs 7 and 8). With solid understanding of the entire spectrum of wave-induced velocities to which *M. flaccida* is exposed, predictions of fatigue breakage were possible, and such predictions successfully accounted for much of *M. flaccida*'s breakage in the field (Fig. 9).

LIST OF SYMBOLS

The equation in which each symbol is first used is given, where applicable.

a	fitted constant, Eqn 2
A	representative area (single-sided surface area for algal frond), Eqn 3
A_{xs}	cross-sectional area of frond resisting drag, Eqn 4
b	fitted constant, Eqn 5
C_D	drag coefficient, Eqn 3
d	sphere diameter, Eqn 9
D_{cy}	fatigue damage for loading cycle, Eqn 6
D_{tot}	total fatigue damage due to loadings, Eqn 7
F_D	drag force, Eqn 3
H_K	fitted constant, Eqn 1
H_S	offshore significant wave height, Eqn 1
m	fitted constant, Eqn 5
N_{br}	number of cycles to breakage, Eqn 5
$N_{br,cy}$	number cycles to breakage at cycle's maximal stress, Eqn 6
Re	Reynolds number, Eqn 8
sd_R	standard deviation of residuals
S_D	stress due to drag, Eqn 4
S_{max}	maximal stress imposed in each loading cycle, Eqn 5
u	fluid velocity, Eqn 3
u_{asym}	fitted constant, Eqn 1
u_{max}	maximal wave-imposed velocity, Eqn 1
u_p	peak velocity, Eqn 10
$u_{p,max}$	day's maximal peak velocity, Eqn 10
$u_{p,norm}$	normalized peak velocity, Eqn 10
ν	kinematic viscosity, Eqn 9
ρ	fluid density, Eqn 3

ACKNOWLEDGEMENTS

Kathy Ann Miller provided important expertise related to the biology of *Mazzaella flaccida*. This research was supported by a Stanford Interdisciplinary Graduate Fellowship to K.J.M., NSF grant IOS-0641068 to M.W.D., and by PISCO, the Partnership for Interdisciplinary Studies of Coastal Oceans, a consortium funded by the Gordon and Betty Moore Foundation and the David and Lucile Packard Foundation. This is contribution 390 of PISCO.

REFERENCES

Abbot, I. A. and Hollenberg, G. J. (1976). *Marine Algae of California*. Stanford, CA: Stanford University Press.

Apt, K. E. (2004). Effects of the symbiotic red alga *Hypneocolax stellaris* on its host *Hypnea musciformis* (Hypneaceae, Gigartinales). *J. Phycol.* **20**, 148-150.

Bell, E. C. and Denny, M. W. (1994). Quantifying "wave exposure": a simple device for recording maximum velocity and results of its use at several field sites. *J. Exp. Mar. Biol. Ecol.* **181**, 9-29.

Boller, M. L. and Carrington, E. (2006a). *In situ* measurements of hydrodynamic forces imposed on *Chondrus crispus* Stackhouse. *J. Exp. Mar. Biol. Ecol.* **337**, 159-170.

Boller, M. L. and Carrington, E. (2006b). The hydrodynamic effects of shape and size change during reconfiguration of a flexible macroalga. *J. Exp. Biol.* **209**, 1894-1903.

Buschmann, A. H., Correa, J. A., Beltrán, J. and Retamales, C. A. (1997). Determinants of disease expression and survival of infected individual fronds in wild populations of *Mazzaella laminarioides* (Rhodophyta) in central and southern Chile. *Mar. Ecol. Prog. Ser.* **154**, 269-280.

Carrington, E. (1990). Drag and dislodgment of an intertidal macroalga: consequences of morphological variation in *Mastocarpus papillatus* Kützing. *J. Exp. Mar. Biol. Ecol.* **139**, 185-200.

Correa, J. A., Flores, V. and Garrido, J. (1994). Green patch disease in *Iridaea laminarioides* (Rhodophyta) caused by *Endophyton* sp. (Chlorophyta). *Dis. Aquat. Org.* **19**, 203-213.

Denny, M. W. (1988). *Biology and the Mechanics of the Wave-Swept Environment*. Princeton: Princeton University Press.

Denny, M. W. (2006). Ocean waves, nearshore ecology, and natural selection. *Aquat. Ecol.* **40**, 439-461.

Denny, M. and Gaylord, B. (2002). The mechanics of wave-swept algae. *J. Exp. Biol.* **205**, 1355-1362.

Denny, M. and Wethey, D. (2001). Physical processes that generate patterns in marine communities. In *Marine Community Ecology* (ed. M. D. Bertness, S. D. Gaines and M. E. Hay), pp. 3-37. Sunderland: Sinauer Associates.

Denny, M. W., Gaylord, B. P. and Cowen, E. A. (1997). Flow and flexibility: II. The roles of size and shape in determining wave forces on the bull kelp *Nereocystis luetkeana*. *J. Exp. Biol.* **200**, 3165-3183.

Denny, M. W., Miller, L. P., Stokes, M. D., Hunt, L. J. H. and Helmuth, B. S. T. (2003). Extreme water velocities: Topographical amplification of wave-induced flow in the surf zone of rocky shores. *Limnol. Oceanogr.* **48**, 1-8.

Dudgeon, S. R. and Johnson, A. S. (1992). Thick vs. thin: thallus morphology and tissue mechanics influence differential drag and dislodgment of two co-dominant seaweeds. *J. Exp. Mar. Biol. Ecol.* **165**, 23-43.

Dudgeon, S. R., Steneck, R. S., Davison, I. R. and Vadas, R. L. (1999). Coexistence of similar species in a space-limited intertidal zone. *Ecol. Monogr.* **69**, 331-352.

Dugan, J. E., Hubbard, D. M., McCrary, M. D. and Pierson, M. O. (2003). The response of macrofauna communities and shorebirds to macrophyte wrack subsidies on exposed sandy beaches of southern California. *Estuar. Coast. Shelf Sci.* **58S**, 25-40.

Dyck, L. J. and DeWreede, R. E. (1995). Patterns of seasonal demographic change in the alternate isomorphic stages of *Mazzaella splendens* (Gigartinales, Rhodophyta). *Phycologia* **34**, 390-395.

Dyck, L. J. and DeWreede, R. E. (2006a). Reproduction and survival in *Mazzaella splendens* (Gigartinales, Rhodophyta). *Phycologia* **45**, 302-310.

Dyck, L. J. and DeWreede, R. E. (2006b). Seasonal and spatial patterns of population density in the marine macroalga *Mazzaella splendens* (Gigartinales, Rhodophyta). *Phycol. Res.* **54**, 21-31.

Faugeron, S., Martínez, E. A., Sánchez, P. A. and Correa, J. A. (2000). Infectious diseases in *Mazzaella laminarioides* (Rhodophyta): estimating the effect of infections on host reproductive potential. *Dis. Aquat. Org.* **42**, 143-148.

Foster, M. S. (1982). Factors controlling the intertidal zonation of *Iridaea flaccida* (Rhodophyta). *J. Phycol.* **18**, 285-294.

Friedland, M. T. and Denny, M. W. (1995). Surviving hydrodynamic forces in a wave-swept environment: consequences of morphology in the feather boa kelp, *Egregia menziesii* (Turner). *J. Exp. Mar. Biol. Ecol.* **190**, 109-133.

Gaylord, B. (1999). Detailing agents of physical disturbance: wave-induced velocities and accelerations on a rocky shore. *J. Exp. Mar. Biol. Ecol.* **239**, 85-124.

Gaylord, B. (2000). Biological implications of surf-zone flow complexity. *Limnol. Oceanogr.* **45**, 174-188.

Gaylord, B., Blanchette, C. A. and Denny, M. W. (1994). Mechanical consequences of size in wave-swept algae. *Ecol. Monogr.* **64**, 287-313.

Hale, B. (2001). Macroalgal materials: foiling fracture and fatigue from fluid forces. PhD thesis, Stanford University, CA, USA.

Hansen, J. E. and Doyle, W. T. (1976). Ecology and natural history of *Iridaea cordata* (Rhodophyta; Gigartinaceae): population structure. *J. Phycol.* **12**, 273-278.

Helmuth, B. and Denny, M. W. (2003). Predicting wave exposure in the rocky intertidal zone: do bigger waves always lead to larger forces? *Limnol. Oceanogr.* **48**, 1338-1345.

Johnson, A. S. (2001). Drag, drafting, and mechanical interactions in canopies of the red alga *Chondrus crispus*. *Biol. Bull.* **201**, 126-135.

Johnson, A. S. and Koehl, M. A. R. (1994). Maintenance of dynamic strain similarity and environmental stress factor in different flow habitats: thallus allometry and material properties of a giant kelp. *J. Exp. Biol.* **195**, 381-410.

Kitzes, J. A. and Denny, M. W. (2005). Red algae respond to waves: morphological and mechanical variation in *Mastocarpus papillatus* along a gradient of force. *Biol. Bull.* **208**, 114-119.

Koehl, M. A. R. and Alberte, R. S. (1988). Flow, flapping, and photosynthesis of *Nereocystis luetkeana*: a functional comparison of undulate and flat blade morphologies. *Mar. Biol.* **99**, 435-444.

Lastra, M., Page, H. M., Dugan, J. E., Hubbard, D. M. and Rodil, I. F. (2008). Processing of allochthonous macrophyte subsidies by sandy beach consumers: estimates of feeding rates and impacts on food resources. *Mar. Biol.* **154**, 163-174.

Liebezeit, G., Wöstmann, R. and Wolters, S. (2008). Allochthonous organic matter as carbon, nitrogen and phosphorous source on a sandbank island (Kachelotplate, Lower Saxonian Wadden Sea, Germany). *Senckenbergiana maritima* **38**, 153-161.

Mach, K. J. (2009). Mechanical and biological consequences of repetitive loading: crack initiation and fatigue failure in the red macroalga Mazzaella. *J. Exp. Biol.* **212**, 961-976.

Mach, K. J., Nelson, D. V. and Denny, M. W. (2007a). Review. Techniques for predicting the lifetimes of wave-swept macroalgae: a primer on fracture mechanics and crack growth. *J. Exp. Biol.* **210**, 2213-2230.

Mach, K. J., Hale, B. B., Denny, M. W. and Nelson, D. V. (2007b). Death by small forces: a fracture and fatigue analysis of wave-swept macroalgae. *J. Exp. Biol.* **210**, 2231-2243.

May, G. (1986). Life history variations in a predominantly gametophytic population of *Iridaea cordata* (Gigartinaceae, Rhodophyta). *J. Phycol.* **22**, 448-455.

Miner, M. A. (1945). Cumulative damage in fatigue. *J. Appl. Mech.* **12**, A159-A164.

Orr, M., Zimmer, M., Jelinski, D. E. and Mews, M. (2005). Wrack deposition on different beach types: spatial and temporal variation in the pattern of subsidy. *Ecology* **86**, 1496-1507.

Rossi, F. and Underwood, A. J. (2002). Small-scale disturbance and increased nutrients as influences on intertidal macrobenthic assemblages: experimental burial of wrack in different intertidal environments. *Mar. Ecol. Prog. Ser.* **241**, 29-39.

Ruxton, G. D. (2006). The unequal variance *t*-test is an underused alternative to Student's *t*-test and the Mann-Whitney *U* test. *Behav. Ecol.* **17**, 688-690.

Seymour, R. J., Tegner, M. J., Dayton, P. K. and Parnell, P. E. (1989). Storm wave induced mortality of giant kelp, *Macrocystis pyrifera*, in Southern California. *Estuar. Coast. Shelf Sci.* **28**, 277-292.

Shaughnessy, F. J. and DeWreede, R. E. (2001). Size, survival and the potential for reproduction in transplants of *Mazzaella splendens* and *M. linearis* (Rhodophyta). *Mar. Ecol. Prog. Ser.* **222**, 109-118.

Shaughnessy, F. J., DeWreede, R. E. and Bell, E. C. (1996). Consequences of morphology and tissue strength to blade survivorship of two closely related Rhodophyta species. *Mar. Ecol. Prog. Ser.* **136**, 257-266.

Shigley, J. E. and Mischke, C. R. (2001). *Mechanical Engineering Design*, 6th edn. San Francisco: McGraw-Hill.

Tomanek, L. and Helmuth, B. (2002). Physiological ecology of rocky intertidal organisms: a synergy of concepts. *Int. Comp. Biol.* **42**, 771-775.

Utter, B. D. and Denny, M. W. (1996). Wave-induced forces on the giant kelp *Macrocystis pyrifera* (Agardh): field test of a computational model. *J. Exp. Biol.* **199**, 2645-2654.

Vogel, S. (1984). Drag and flexibility in sessile organisms. *Am. Zool.* **24**, 37-44.